


SCIENTIFIC REPORTS



OPEN

Trading off stability against activity in extremophilic aldolases

Markus Dick¹, Oliver H. Weiergräber², Thomas Classen³, Carolin Bisterfeld¹, Julia Bramski¹, Holger Gohlke⁴ & Jörg Pietruszka^{1,3}

Received: 17 August 2015

Accepted: 06 November 2015

Published: 19 January 2016

Understanding enzyme stability and activity in extremophilic organisms is of great biotechnological interest, but many questions are still unsolved. Using 2-deoxy-D-ribose-5-phosphate aldolase (DERA) as model enzyme, we have evaluated structural and functional characteristics of different orthologs from psychrophilic, mesophilic and hyperthermophilic organisms. We present the first crystal structures of psychrophilic DERAs, revealing a dimeric organization resembling their mesophilic but not their thermophilic counterparts. Conversion into monomeric proteins showed that the native dimer interface contributes to stability only in the hyperthermophilic enzymes. Nevertheless, introduction of a disulfide bridge in the interface of a psychrophilic DERA did confer increased thermostability, suggesting a strategy for rational design of more durable enzyme variants. Constraint network analysis revealed particularly sparse interactions between the substrate pocket and its surrounding α -helices in psychrophilic DERAs, which indicates that a more flexible active center underlies their high turnover numbers.

Enzymes from thermophilic organisms are of particular interest to biotechnology due to their adaptation to high temperatures^{1,2}. As a result, considerable effort is being put into screening for new, thermophilic enzyme variants. An alternative route is to re-design proteins from mesophilic organisms, increasing their thermostability. However, rational identification of hotspots affecting enzyme stability is still a challenging task and is based on sophisticated knowledge on structural determinants responsible for thermostability. In recent years, many new protein structures from meso- and thermophilic organisms have been determined, and large genome libraries from a variety of species have been compiled³. Aside from well-known stabilizing features such as hydrophobic cores, disulfide and salt bridges⁴, enzymes can be stabilized by strengthening intermolecular interactions in oligomeric structures^{5,6}. However, compared to other stabilizing factors, the properties of oligomeric interfaces have received minor attention in studies dealing with adaptation to high temperature.

Thermal adaptation has also evolved to low temperatures. Psychrophilic organisms have developed many modulations on a cellular and molecular level to survive under those extreme conditions. While the high catalytic activity and broad substrate spectrum of most psychrophilic enzymes make them attractive tools for biotechnology^{7–9}, their industrial application is hampered by their short life-times under typical fermentation conditions. Structural characteristics of these proteins include clusters of glycine residues and a reduced number of charged and hydrophobic side chains¹⁰. However, due to the low number of available 3D structures (<100 Protein Data Base-PDB-entries containing "psychrophilic" or "cold-adapted" in October 2015), aspects of the structural origin of low-temperature adaptation are awaiting further investigation.

The 2-deoxy-D-ribose-5-phosphate aldolase (DERA) is an enzyme involved in nucleotide catabolism¹¹. As it is found in all kingdoms of life, including psychrophilic and hyperthermophilic organisms,

¹Institute of Bioorganic Chemistry, Heinrich-Heine-Universität Düsseldorf im Forschungszentrum Jülich, and Bioeconomy Science Center (BioSC), Jülich, Germany. ²Institute of Complex Systems ICS-6: Structural Biochemistry, Forschungszentrum Jülich GmbH, Jülich, Germany. ³Institute of Bio- and Geosciences IBG-1: Biotechnology, Forschungszentrum Jülich GmbH, Jülich, Germany. ⁴Institute of Pharmaceutical and Medicinal Chemistry, Heinrich-Heine-Universität Düsseldorf, Düsseldorf, Germany. Correspondence and requests for materials should be addressed to H.G. (email: gohlke@uni-duesseldorf.de) or J.P. (email: j.pietruszka@fz-juelich.de).

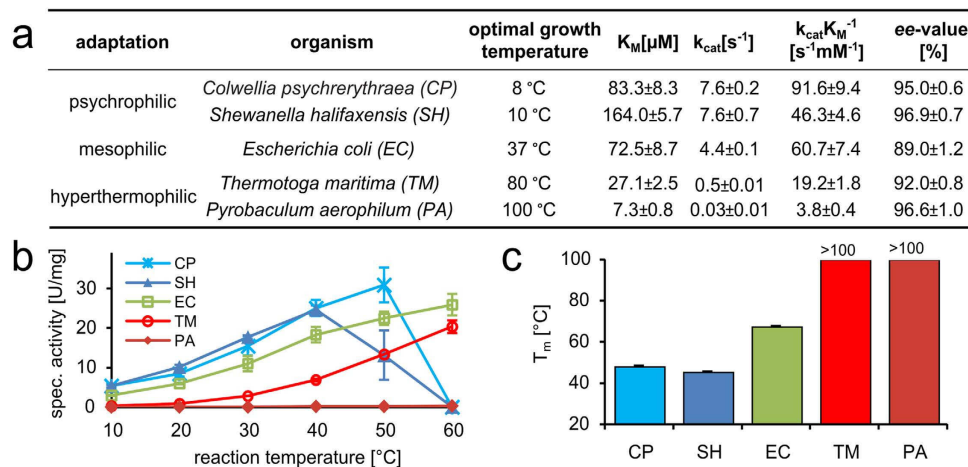


Figure 1. Kinetic and biophysical properties of DERAs used in this study. (a) Overview of all used DERA orthologs with optimal growth conditions of their hosts^{57–60}, Michaelis-Menten parameters obtained from steady-state kinetics and enantiomeric excess (*ee*) of the conversion of propanal and acetaldehyde to (*R*)-3-hydroxy-pentanal. (b) Specific activity at different reaction temperatures. (c) Melting temperatures have been obtained by CD spectroscopy at 222 nm. All error bars represent the standard deviation.

it represents a suitable model system for studying adaptation to extreme temperatures. The enzyme catalyzes the formation of C-C bonds between an aldehyde as an electrophile and acetaldehyde as a nucleophile in a highly stereoselective manner¹². Thus, it has become an important alternative to chemical methods to synthesize chiral building blocks for natural products^{13,14}. During the past decade, four crystal structures of hyperthermophilic DERAs were solved^{15–17}, but thus far no structure of psychrophilic origin is available.

Here we present comparative biochemical, structural, and computational studies of DERAs from psychrophilic, mesophilic and thermophilic organisms. In order to establish a solid foundation for further experiments, we have determined the first crystal structures of DERAs derived from cold-adapted organisms. Properties affecting the stability against thermal inactivation are investigated with a deliberate focus on the role of the dimer interface. Finally, we show likely reasons for the very different biophysical characteristics of DERAs from psychrophilic vs. mesophilic organisms.

Results

Biochemical characterization. Different DERA orthologs from psychrophilic (*Colwellia psychrerythraea*, *Shewanella halifaxensis*), mesophilic (*Escherichia coli*) and hyperthermophilic (*Pyrobaculum aerophilum*, *Thermotoga maritima*) organisms were used for this study (Fig. 1a). DERAs from psychrophilic organisms have not been characterized until now. After cloning, expression and purification, pure (>95%) and active enzymes from all organisms were obtained. Initially, biochemical and biophysical characteristics of all five DERA orthologs were compared (Fig. 1). The DERA-catalyzed aldol reaction between acetaldehyde and propanal to 3-hydroxy-pentanal showed a high enantiomeric excess (89–96%) for the (*R*)-enantiomer in all cases. Clear differences in terms of activity and stability were determined. Both K_M and k_{cat} values decrease with increasing optimal growth temperature of the organism (details on the Michaelis-Menten data are provided as Supplementary Fig. S1a–c).

For all enzymes specific activity shows a steady increase with temperature (Fig. 1b), until the melting-range (Fig. 1c) is reached. This is at variance with previous reports for enzymes from psychrophilic organisms, where activity was shown to already drop at lower temperatures⁹. Due to the short reaction time of 1 min, time-dependent denaturation is delayed in this assay. This explains why DERA_{CP} displays a temperature optimum above its melting point. Between 10 and 60 °C, DERA_{PA} does not exhibit a specific activity higher than 1.5% that of DERA_{EC}. Overall, our biochemical data of DERA_{EC}, DERA_{TM} and DERA_{PA} are in agreement with those from Sakuraba *et al.*¹⁷. Stabilities of all DERA orthologs were determined with both CD spectroscopy (Fig. 1c, an example spectrum for T_m determination is shown in Supplementary Fig. S1d,e) and an activity-based assay (Supplementary Fig. S1f). DERAs from psychrophilic species had a similar thermostability and were around 20 K less stable than DERA_{EC}. No melting point could be identified for hyperthermophilic DERAs, thus it must exceed 100 °C in both cases. However, when incubated at 100 °C, only DERA_{PA} was stable over night at that temperature, while DERA_{TM} had a half-life of 22 min. These observations prompted us to investigate structural reasons for the diverse properties found with DERAs of different thermal adaptation.

Crystallization of psychrophilic DERAs. As no structure was available for any psychrophilic DERA, crystallization trials were performed, and protein crystals suitable for diffraction experiments were

obtained. The X-ray structures of both psychrophilic DERAs were determined with resolutions of 2.1 Å for *C. psychrerythraea* and 1.8 Å for *S. halifaxensis* (Supplementary Table S1). Superposition of the structures with those of meso- and hyperthermophilic DERAs revealed a high similarity of the monomeric units, with root-mean-square (r.m.s.) deviations (RMSD) in the range of 0.63–1.65 Å (Supplementary Fig. S2). In view of this high structural similarity, it is interesting to note that the sequence identity between hyperthermophilic and meso-/psychrophilic DERAs is quite low (29–31%, see Supplementary Fig. S2). Nevertheless, the conservation of all catalytically important residues (e.g., K167 and D102, numbering according to *E. coli* DERA) together with a virtually identical fold strongly suggests a common evolutionary origin of all five DERA orthologs. The structures display a canonical TIM barrel fold built up of eight β - α repeats in a toroidal arrangement, with an additional N-terminal helix (α 0) directly adjacent to the C-terminal helix α 8 (vide infra). Furthermore, all DERAs investigated in this study form constitutive dimers. We note that the relative orientations of protomers as well as the characteristics of the dimer interface for both psychrophilic DERAs closely resemble the situation in the mesophilic (*E. coli*) enzyme. In contrast, hyperthermophilic aldolases have evolved a different dimeric arrangement (discussed below). Comparing the substrate binding pockets of the new structures with DERA_{EC}, no amino acid exchanges or significant conformational differences were found within a radius of 5 Å about the natural substrate (as represented by the covalent intermediate included in PDBID 1JCL¹²). With the 3D structures of all five DERAs at hand, sophisticated structure-based studies such as rational enzyme design and computational investigations could be performed.

Structural features related to thermostability. To identify the structural properties underlying the stabilization effects in hyperthermophilic DERAs and the increased catalytic efficiency of psychrophilic DERAs, we set out to quantify inter- and intramolecular interactions by *in silico* methods (PDB IDs used for computational studies are given in Supplementary Table S2). Our initial strategy was to determine the number and strength of non-covalent interactions (hydrogen bonds, salt bridges, and hydrophobic contacts) in the crystal structures using the FIRST software¹⁸, which did not give a satisfying result as there was no correlation between the calculated number of hydrogen bonds/salt bridges and measures of thermostability (Supplementary Table S3). For hydrophobic interactions, an R^2 of 0.91 was determined, suggesting a correlation between thermostability and the number of hydrophobic contacts. However, the number of hydrophobic contacts does not allow differentiating between DERA_{SH} and DERA_{EC}, or between the two hyperthermophilic DERAs, although these two proteins clearly differ in thermostability. The quantification of non-covalent interactions in ensembles of conformations generated by 3×50 ns molecular dynamics (MD) simulations could partly improve R^2 in the case of hydrogen bonds and salt bridges (Supplementary Table S3), but good correlations ($R^2 \geq 0.8$) were only obtained if the strongest and least frequent hydrogen bonds and salt bridges were considered. Furthermore, now the number of hydrophobic contacts does not correlate with thermostability ($R^2 = 0.08$). Overall, this outcome shows that purely counting non-covalent interactions yields correlations with thermostability. However, the quality strongly depends on the structural origin and the particular choice of descriptor. Hence, we hypothesized that, in addition to the frequency, the distribution of the interactions within the protein is important. This hypothesis was probed by constraint network analysis (CNA) recently developed by Pflieger *et al.*¹⁹. Here, a protein is represented as a network of constraints deduced from covalent and non-covalent interactions, from which information on the biomacromolecular flexibility/rigidity is computed²⁰. In CNA, thermal unfolding of a protein is simulated by gradually removing hydrogen bond constraints from the network in the order of increasing strengths²¹. It has been shown that the temperature of the resulting phase transition T_p from a largely rigid to a largely flexible network (which can be also described as a melting point) correlates with measures of thermostability, if proteins from the same structural family are compared^{21,22}. For all five DERA orthologs, three independent MD simulations of 100 ns each were performed. Evaluation of these MD simulations via calculation of the RMSD of C_α atoms with respect to the corresponding starting structure (Supplementary Fig. S3a) and of radii of gyration (Supplementary Fig. S3b) showed that during the simulation time of 100 ns, all protein orthologs remained structurally stable (RMSD mostly < 3.0 Å and standard deviation of the radius of gyration < 2 Å). Furthermore, the r.m.s. inner product (RMSIP) over the first ten principal components²³ shows for respective pairs of independent MD simulations of one ortholog that the conformational subspaces covered by the two MD simulations are similar to highly similar (range of RMSIP values: 0.63 to 0.79; Supplementary Table S4). From these simulations, initially, 1125 conformations in the time range from 5–50 ns were selected, and the T_p -value for each snapshot was calculated via CNA. The frequencies of T_p -values in the ensemble follow a Gaussian distribution in all cases (Supplementary Fig. S4). Note that the calculated T_p -values should be considered relative values because the absolute phase transition temperatures may depend on the architecture and the size of the enzyme¹⁹. To see how robust the CNA results are with respect to the chosen structural ensemble, CNA calculations were repeated for the range of 50–100 ns. To validate the CNA results at the macroscopic level, experimental melting temperatures would be the best measures of thermostability. Unfortunately, a well-defined melting temperature is not available for the hyperthermophilic DERAs (> 100 °C, see Fig. 1c). Thus, we instead used the optimal growth temperature of the source organisms (T_{org}), which has been previously applied to compare meso- and thermophilic proteins^{21,22,24}. T_{org} is an approximate descriptor for protein thermostability as, on average, the value for T_m of a protein is around 24 °C higher than the T_{org} of the corresponding species²⁴.

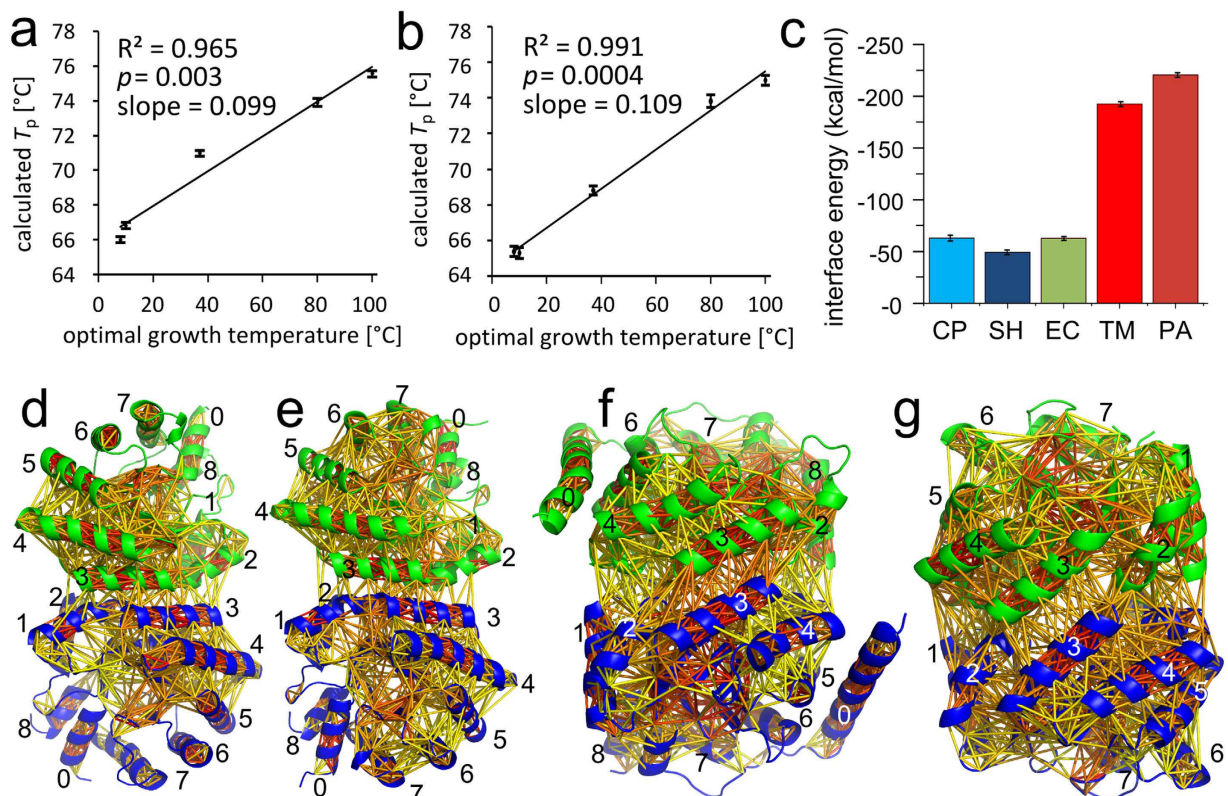


Figure 2. Structural rigidity of DERAs from psychrophilic, mesophilic, and hyperthermophilic organisms, as calculated by CNA. (a,b) Correlation of phase transition temperature T_p computed by CNA over ensembles from MD simulations in the range of (a) 5–50 ns and (b) 50–100 ns with the optimal growth temperature of the host. Error bars represent the standard error of the mean. (c) Sum over energies of all rigid contacts between residue pairs at the dimer interface. (d–g) Visualization of rigid contact strength between amino acid pairs for (d) $DERA_{CP}$ ($DERA_{SH}$ showed a pattern that was nearly identical), (e) $DERA_{EC}$, (f) $DERA_{TM}$, and (g) $DERA_{PA}$. Different orientations of the structures result from the non-equivalent dimer arrangements in psychro-/mesophilic vs. hyperthermophilic DERAs. The strength of the interaction is color coded from yellow (weak) to red (strong).

For evaluation, conformations of all three MD simulations were extracted, and the overall average and standard error of the mean of T_p were calculated for each DERA ortholog (Supplementary Table S5). The computed T_p shows a significant ($p < 0.01$) and very good correlation with T_{org} ($R^2 = 0.965$ (0.991)) over the MD ensemble in the range of 5–50 ns (50–100 ns) (Fig. 2a,b). The range of predicted T_p values is smaller than that of experimental T_{org} , in line with slopes of the correlation lines of ≈ 0.1 . A reason for this may be that the T_p values rely on an empirical relationship introduced previously^{21,25}, which has been determined for a dataset of orthologous meso- and thermophilic protein pairs with T_{org} in the range of 30–83 °C. The deviation indicates that a system-specific reparametrization might be necessary here. The values obtained from individual MD simulations, together with the standard errors of their means, are given in Supplementary Table S5. These results show that the T_p predictions from the individual MD simulations are consistent (maximal spread in T_p values across three trajectories: 3 °C), in line with the above RMSIP analysis. The differences between the computed T_p values for the first and second 50 ns are ≤ 2.2 K in all cases, strongly indicating converged calculations. The results suggest that the model underlying CNA correctly captures differences in the thermostability of the DERAs.

We next analyzed on a per-residue basis how changes in thermostability relate to changes in local structural stability (rigidity). The local structural stability in terms of the strength of rigid contacts was characterized, which describes when two residues cease to reside within one rigid region of the protein during the thermal unfolding simulation^{25,26}. In Fig. 2d–g, the networks of rigid contacts are compared for different DERAs. Qualitatively, the two enzymes from hyperthermophilic organisms have very dense networks that also extend markedly across the dimerization interface. In contrast, DERAs from psychrophilic and mesophilic organisms show much fewer rigid contacts in the interface region. Furthermore, the DERAs in this group differ with respect to the rigid contacts between the outer helices 5–7 and the inner part of the TIM barrel (Fig. 2d,e). To quantify the influence of structural stability in the interface region on the thermostability of the DERAs, we computed the sum over energies of all rigid contacts

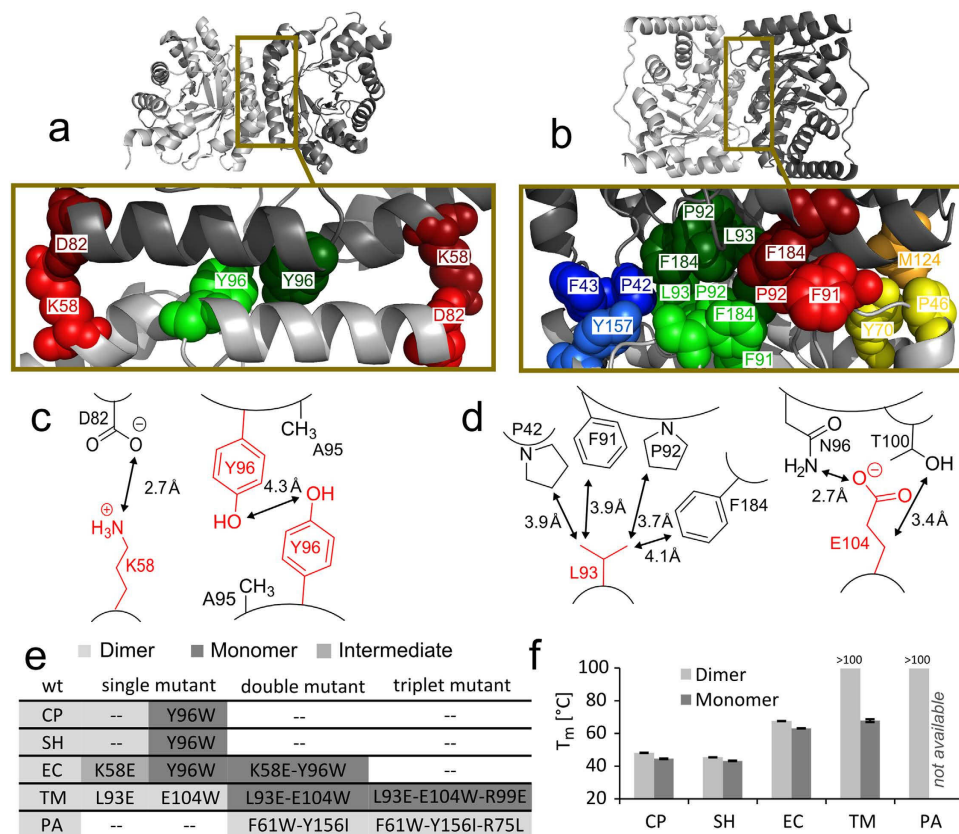


Figure 3. Design of mutants in the dimer interface of DERA orthologs. (a,b) Interactions in the dimer interface of (a) DERA_{EC} and (b) DERA_{TM}. Amino acids belonging to the same pair or cluster are shown in CPK mode with similar colors. (c,d) Schematic representation of regions in (c) DERA_{EC} and (d) DERA_{TM} that were selected for modification. Mutated amino acids are labeled in red. (e) Overview of all designed mutants and their oligomeric states. Positionally equivalent sites are listed in the same column. (f) Stability of dimeric and monomeric DERAs from different organisms. Melting temperatures (with standard deviation) have been obtained by CD spectroscopy at 222 nm.

between residue pairs at the dimer interface (Fig. 2c). The more negative this value, the more stable is the interface region. The results indicate that the interface regions of DERA_{TM} and DERA_{PA} are much more structurally stable than those of their mesophilic and psychrophilic counterparts.

Design of monomeric DERAs. By comparing the structures of DERA_{EC}, DERA_{TM} and DERA_{PA}, Sakuraba *et al.* proposed that hydrophobic clusters within the dimer interface (Fig. 3a,b) strongly contribute to the overall thermostability of hyperthermophilic DERAs¹⁷. Our CNA results support the hypothesis of stronger interactions in the dimer interfaces of the thermostable DERAs. In order to verify these findings with *in vitro* experiments, DERA mutants were designed with the intention to weaken the affinity between monomeric subunits. Two different strategies were followed: Either a charged or hydrophobic interaction partner was mutated to generate a repulsive interaction (e.g., by a K58E mutation, which should repel D82), or a sterically demanding group such as a tryptophan was introduced, disturbing shape complementarity at the interface (Fig. 3c,d). Size exclusion chromatography was used to analyze the hydrodynamic sizes of the mutant proteins (an example is shown in Supplementary Fig. S5). Soluble and active monomeric variants for DERAs from *C. psychrerythraea*, *S. halifaxensis*, *E. coli* and *T. maritima* have been created following this methodology; specific mutations are denoted in Fig. 3e, together with the resulting oligomeric state. For the K58E-mutant of DERA_{EC}, the hydrodynamic size was in between the values of the monomer and the dimer. Thus, it might feature a dynamic equilibrium between both states. Strikingly, DERA from *P. aerophilum* retained its original oligomeric state even after introducing a triple mutation. It is important to note that for the monomeric variants the specific activity did not change significantly (Supplementary Table S6). This preservation of function is a good indication that the overall structure of the protein has not been affected by altering the oligomeric state. Furthermore, the T_m values of all monomerized DERAs with either psychrophilic or mesophilic origin decreased by only a few Kelvin (Fig. 3f). The same holds true for the activity half-life at elevated temperature (Supplementary Table S6). In contrast, conversion of the hyperthermophilic DERA from

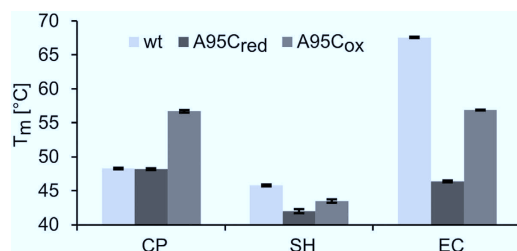


Figure 4. Melting points of oxidized and reduced forms of A95C mutants vs. wt enzymes. The numbering corresponds to DERA_{EC}. Melting temperatures have been obtained by CD spectroscopy at 222 nm. Error bars represent the standard deviation.

T. maritima to a monomer decreased its stability by more than 30 K. These results provide experimental support for the hypothesis of Sakuraba and co-workers¹⁷. While dimerization via the native interface is not important for the stability of meso- and psychrophilic DERAs, the much more extensive interactions in the *T. maritima* variant appear to be an essential determinant of thermal stability.

Stabilizing the dimer interface. We were able to destabilize a hyperthermophilic DERA by disturbing the interaction network between the monomeric subunits. For use in biotechnology, however, the converse approach, i.e., ways of stabilizing enzymes, is of particular interest. Hence, the finding that strong intermolecular interactions may promote thermostability inspired an attempt to enhance the interfacial interaction of DERAs from *C. psychrerythraea*, *S. halifaxensis*, and *E. coli*. Introducing a novel hydrophobic cluster similar to those found in both hyperthermophilic DERAs is a possible strategy. However, this approach would imply extensive mutations increasing the risk of negative side effects (influence on expression level, specific activity, and stability). Therefore, an artificial disulfide bridge was introduced because this is the only covalent (except for rare isopeptide bonds) and thus the strongest interaction between two non-neighboring residues in a protein. According to the empirical rules proposed by Hazed *et al.*²⁷, the distances between C_β-atoms of both protein chains were determined, and all pairs (excluding prolines) with a distance of 3.83 ± 0.18 Å were selected. For all three non-hyperthermophilic DERAs one pair was found: A95–A95. As this position is located close to the C2 axis, only one mutation is necessary to provide both cysteines for the new disulfide bridge. After expression and purification of the A95C mutants, formation of the disulfide bridge was verified via SDS-PAGE under non-reducing conditions (only the oxidized mutant led to a 56 kDa band on the gel). The stability of all variants was tested by CD spectroscopy (Fig. 4). In the reduced state (i.e., without formation of the disulfide bridge), the A95C mutation turned out to negatively affect the stability of DERA_{SH} and DERA_{EC}, but did not influence the stability of DERA_{CP}. It remains unclear why in two out of three cases the A95C mutation has a negative effect on thermostability. However, these results are not surprising as studies have shown that more than 80% of all single point mutations in a protein decrease its stability²⁸. Importantly, oxidation of the Cys residues in the disulfide bridge results in an increased thermostability in the case of all three proteins. While in DERA_{SH} and DERA_{EC} the melting point of the oxidized form was still lower than the wt value, the exchange led to a marked increase of 8.4 K in thermostability in the case of DERA_{CP}. Further tests for the DERA_{CP}-A95C_{ox} variant revealed a much longer half-life at 50 °C (>80 min vs. 1 min for the wt) and $86 \pm 8\%$ of the wt activity. Overall, the results demonstrate that it is possible to increase the thermal stability of a non-thermophilic DERA by strengthening the interactions at the dimer interface.

Features promoting activity in psychrophilic DERAs. Our CNA data did not reveal major differences in the structural stabilities of the dimer interfaces of meso- and psychrophilic DERAs. Thus, experimental differences in thermostability and activity parameters (Fig. 1) most probably arise from differences in the type and strength of intramolecular interactions in these proteins. Along these lines, CNA suggested a varying density of rigid contacts between secondary structure elements (Fig. 2d–e). To further investigate this aspect, the sum over energies of rigid contacts connecting each α -helix or β -strand to the rest of the protein was computed (Fig. 5a,b). In all three DERAs, the β -strands are connected more strongly to other protein parts than the helices. Comparing DERA_{EC} with DERA_{CP} and DERA_{SH}, no difference can be seen between corresponding β -strands. In contrast, helices 5 and, particularly, 6 and 7 show markedly reduced strengths of rigid contacts in the psychrophilic enzymes. These helices are placed directly opposite to the dimer interface (Fig. 5c), next to strands 6 and 7 containing the catalytically active K167 (Schiff base formation, numbering corresponds to DERA_{EC}) and K201 (pK_a reduction of the active lysine), respectively.

This finding suggests a possible explanation why both DERAs from psychrophilic organisms have a higher catalytic activity than their mesophilic (and thermophilic) counterparts at comparable temperatures: A weaker connection to the outer helices implies a higher mobility of the adjacent β - α loops, which decorate the “catalytic face” of the TIM barrel fold. Since these loops contribute to both the substrate channel and the active center^{29,30}, they are thought to modulate both catalytic specificity and

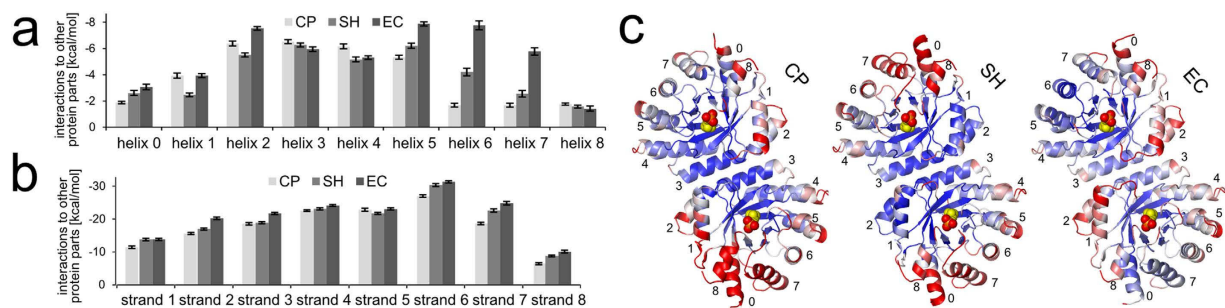


Figure 5. Comparison of structural stability and mobility in secondary structure elements of psychro- and mesophilic DERAs. (a,b) Sum over energies of rigid contacts between residues of each (a) α -helix and (b) β -strand of DERA_{EC}, DERA_{CP} and DERA_{SH} and the rest of the protein without the respective secondary structure element as computed by CNA. The values are divided by the number of amino acids in the secondary structure element and thus represent an average value with standard error. (c) Relative B-factor distribution from blue (mean – SD) to red (mean + SD). The natural substrate is represented in CPK mode (phosphate group in red/orange, other atoms in yellow). For DERA_{EC}, PDBID 1JCL¹² has been used.

rate of conversion. Indeed, mutations in the outer helices as well as the β - α loops have been previously demonstrated to increase the activity of a hyperthermophilic indole-3-glycerol phosphate synthase (TrpC) at low temperatures³¹. Kinetic data indicated that these mutations result in an increased rate of product release, presumably due to enhanced flexibility and reduced affinity of the phosphate binding site (which is also present in DERAs). Further support for this view is provided by X-ray crystallography. In structure refinement, B-factors are used to parameterize coordinate uncertainty, which is largely related to thermal motion on different scales. The relative B-factor distribution of the backbone atoms reveals a tendency towards increased flexibility in helices 0, 6, and 7 of the psychrophilic DERAs, compared to DERA_{EC} (Fig. 5c). A similar trend is observed for the respective β - α loops, particularly in the segments immediately preceding the helices. Hence, our X-ray structures provide independent clues in favor of the hypothesis that adaption to low temperatures in psychrophilic DERAs involves a more flexible environment of the substrate binding pocket.

Discussion

In our studies we used 2-deoxy-D-ribose-5-phosphate aldolase (DERA) as a model enzyme to elucidate mechanisms of thermal adaptation of orthologs from psychrophilic (*C. psychrerythraea*, *S. halifaxensis*), mesophilic (*E. coli*) and hyperthermophilic (*T. maritima*, *P. aerophilum*) organisms. The biochemical characterization revealed two general trends: On the one hand, the catalytic efficiency decreases with increasing temperature of adaption while maintaining the enantioselectivity. On the other hand, the thermostability increases with optimal growth temperature of the source organism. Sakuraba *et al.*¹⁷ hypothesized that interactions in the dimeric interface play a major role in thermal adaptation of DERA_{TM} and DERA_{PA}. We tested this assumption by creating mutants of all five DERAs resulting in formation of monomers rather than the (wildtype) dimers. While stability of DERAs from psychrophilic and mesophilic sources was not influenced significantly, stability of DERA from the thermophile *T. maritima* was severely reduced. This supports the hypothesis of the dimer interface as a stability determinant in thermostable proteins, but the concept does not extend to the native dimers of mesophilic and psychrophilic DERAs. Nevertheless, by installing a disulfide bridge in the interface of DERA_{CP} as a psychrophilic representative, the melting temperature could be increased. The result is in agreement with other studies conducted with unrelated proteins where either by *in vitro* evolution³² or by rational design^{33,34} thermal stability could be increased upon introduction of intermolecular disulfide bridges. Research in the Protein Data Bank showed that 61% of all protein entries indicate more than one chain in their biological units. Several reasons for protein oligomerization like regulation, reduction of genomic size and adaptation of particle concentration are known³⁵. Most of these are directly related to the protein's *in vivo* function. Enzymes in biotechnology are typically overexpressed for *in vitro* applications. Thus, as they still form oligomers, mutations to stabilize the interface can be utilized to enhance thermostability in mesophilic enzymes.

Adding to our mutational study, computational analyses by means of CNA revealed a differing extent of interface interactions. In the case of psychrophilic DERAs, no structural information was available prior to this study. The first two psychrophilic DERA structures presented here reveal that the inner sphere of the active site does not differ significantly from DERA_{EC}. Hence, the reason for their increased catalytic efficiency must reside in the outer shell. CNA calculations as well as a B-factor analysis were indeed able to identify distinctive features. Specifically, patches of higher flexibility were detected in the area of β - α repeats 6 and 7, caused by weaker interactions between the sheath of helices and the inner β -barrel. This region is located opposite to the dimer interface and contains the catalytically important residues such as the active lysine and the pK_a-lowering lysine. *In vitro* studies on the activity of enzymes

with $(\beta\text{-}\alpha)_8$ -barrel fold already suggested that the region surrounding the binding pocket influences the substrate conversion rate^{31,36}. Our data support the notion that psychrophilic enzymes are structurally more flexible in their active sites, which is an important determinant of overall catalytic performance^{10,37}.

In this study, MD simulations were primarily used for generating structural ensembles for T_p calculations by CNA. However, many other studies on cold-adapted enzymes included MD simulations and thus can be used to put our findings into perspective. Some of these studies showed that global characteristics such as a reduced number of hydrogen bonds³⁸ and salt bridges³⁹ contribute to a higher overall flexibility in certain psychrophilic enzymes. Our investigations on DERAs of different thermal adaptation did not clearly support this view. Other studies revealed that adaptation mostly occurs locally in specific regions: By comparing mesophilic and psychrophilic elastases, Papaleo *et al.* detected flexible loop regions around the binding pocket, which might cause a higher activity of the enzyme^{40,41}, in accordance to what we found for DERAs. While most computational studies were performed with monomeric proteins, Papaleo *et al.* also analyzed intermolecular interactions of the dimeric, cold-adapted alkaline phosphatase, revealing a higher flexibility in the interface region, which might be directly related to enzyme reactivity⁴². Notably, for dimeric DERAs, such intermolecular contacts contribute to thermostability, with no influence on activity. In conclusion, intermolecular interactions in extremophilic enzymes can be used both to stabilize the protein at high temperatures and to enhance the catalytic activity in a cold environment and thus can play a key role in thermal adaptation.

When viewed in the broader context of protein evolution, the DERA structures investigated in this study reveal two fundamental strategies used to achieve adaptation to widely differing ambient temperatures. The psychrophilic/mesophilic regime does not require special measures to prevent thermal unfolding and is therefore compatible with a (stability-wise) 'neutral' dimer interface. Nevertheless, dynamic properties of the catalytic center (and possibly other parts of the structure) still need to be adjusted in order to maintain biological activity within favorable bounds; this is achieved in a conservative manner via modulation of the density and strength of interactions between secondary structure elements. This strategy, however, is insufficient when extended into the high-temperature range. In addition to an overall increase in non-covalent interactions, (hyper-)thermophilic DERAs have thus adopted a peculiar dimer assembly with a strong stabilizing effect. A thorough comparison of DERA_{TM} and DERA_{PA} reveals an even tighter constraint network in the latter, in accordance with its higher working temperature, suggesting that adaptation of local stiffness is still relevant in the thermophilic group.

It is interesting to note that *T. maritima* and *P. aerophilum* belong to different kingdoms, the former being a bacterium while the latter is an archaeon. In view of this very distant relationship, the similarity in temperature adaptation of both DERAs (in particular regarding the dimer interface) is remarkable. Related to this observation, one can speculate that (a) this particular type of dimer has been present in a common ancestor of bacteria and archaea, or (b) a primordial gene has been exchanged at a later time by lateral transfer, followed by significant divergence of amino acid sequences, or (c) this particular strategy has emerged independently in the two phyla. While we cannot decide among these options based on our data, it is obvious that this adaptation must have been very stable on the evolutionary time scale.

In summary, this study provides new insights into both the stability of thermophilic (oligomeric) DERAs and the flexibility of their psychrophilic counterparts. In addition to the computational analyses, the concept of modifying the oligomeric state or interaction strength between protomers is important from an application point of view, such as stabilizing proteins for biotechnological applications.

Methods

Cloning, protein expression and purification. DERA-coding deoC-genes from *P. aerophilum*, *T. maritima* and *C. psychrerythraea* were synthesized by GenScript and cloned into the pET21a-vector with a C-terminal 6× His-Tag. The gene from *S. halifaxensis* was isolated from genomic DNA, and the deoC-gene from *E. coli* had been isolated previously⁴³. Single point mutations were inserted via QuikChange (Stratagene) or round-the-horn⁴⁴ mutagenesis with Phusion polymerase (list of primers is shown in Supplementary Table S7) and verified by sequencing (GATC Bio-tech).

All enzymes were expressed in *E. coli* BL21(DE3) strain in TB-medium. Expression was initiated with 0.1 mM IPTG, and after 16 h (24 h for psychrophilic enzymes) incubation at 25 °C (18 °C) cells were harvested (15 min at 7000 × g). For purification 1–4 g cells were resuspended in 5 volumes of 20 mM potassium phosphate (KP_i)-buffer at pH 7, disrupted via sonification, and after centrifugation (15 min at 12000 × g) the supernatant was loaded on a NiNTA-column in a cyclic process (15 min). The column was connected to an ÄKTA purification system and after washing with KP_i-buffer and 20 mM imidazole the enzyme was eluted with 250 mM imidazole. PD-10 desalting columns were used to rebuffer the solution to 20 mM KP_i, and purity was verified with SDS-PAGE. Finally the protein concentration was determined by the Bradford assay⁴⁵. Prior to crystallization screenings and to determine its hydrodynamic radii size exclusion chromatography was used. A SuperdexTM200 10/300 GL (GE Healthcare) column was equilibrated in 100 mM KP_i, 150 mM NaCl (pH 7); 1–5 mg protein was loaded on the column, and the elution profile was recorded by means of absorbance at 280 nm. Five protein standards between 12.5 and 200 kDa were used for calibration (see Supplementary Fig. S5).

Biochemical characterization. The activity for cleavage of the natural substrate 2-deoxy-D-ribose-5-phosphate (DRP) was measured for 1 min and (if not given explicitly) at 25 °C. In a retro-aldol reaction glyceraldehyde-3-phosphate is formed. This is reduced to glycerol-3-phosphate by the auxiliary-enzymes glycerol-3-phosphate dehydrogenase/triose phosphate isomerase (GDH/TPI) under NADH-consumption, which was detected with a photometer at 340 nm. The standard reaction mix (400 µl) contained 0.4 mM DRP, 0.15 mM NADH, 4 U GDH, 11 U TPI and 10 µl DERA solution.

Circular dichroism (CD) spectroscopy was used to determine the melting points of the proteins. The minimum of the far-UV spectrum at 222 nm was used to quantitate the folding of the proteins at different temperatures. A range from 25 °C to 100 °C was used with a heating rate of 1 °C/min. The molar ellipticity was plotted against temperature, resulting in a sigmoid curve, and the inflection point was used as the melting point.

Determination of enantiomeric excess for a DERA-catalyzed aldol reaction between acetaldehyde and propanal. The aldol reaction was performed in analytical scale, followed by a derivatization with 2,4-DNPH. The products were extracted and analyzed by chiral HPLC. The DERA reaction was performed in 2 ml tubes. 28 µl of a stock solution containing 7 µl of propanal (0.10 mmol), 7 µl of acetaldehyde (0.12 mmol, 1.3 eq.) and 14 µl dimethyl sulfoxide (0.2 mmol, 2.0 eq.) were added to 0.5 ml of triethanolamine buffer (0.1 M, pH 7). After addition of 20 µl enzyme solution (cell free crude extract), the solutions were shaken at 25 °C and 200 rpm for 16 h. For derivatization a solution of 40 mg DNPH (0.2 mmol) and 7 µl conc. HCl (0.31 mmol) in 0.5 ml dimethyl sulfoxide was added to the DERA reaction. After stirring for 2 h at 50 °C, 300 rpm, the products were extracted with 600 µl of ethyl acetate. A short centrifugation led to good phase separation. 450 µl of the organic phase were transferred to another tube and dried over MgSO₄ to avoid water contamination. After another short centrifugation step, 350 µl were transferred into new tubes. The organic phase was removed in a vacuum centrifuge. The residues were dissolved in 90:10 *n*-heptane/2-propanol-mixtures. To remove unsolved compound a short centrifugation was necessary. The clear yellow supernatant was then used to analyze the enantiomeric composition of the products by means of chiral HPLC: Chiralpak IA, 0.5 ml·min⁻¹, 80:20 *n*-heptane:*i*PrOH, 345 nm: (*R,E*)-1-[2-(2,4-Dinitrophenyl)hydrazono]pentan-3-ol $t_R = 70.9$, (*S,E*)-1-[2-(2,4-Dinitrophenyl)hydrazono]pentan-3-ol $t_S = 79.0$.

Synthesis of reference compounds. Details on the synthesis of the reference compounds as well as general information for chemical reactions are described in Supplementary Methods. A reaction schema is provided in Supplementary Fig. S6.

Protein crystallization. Screening for crystallization conditions of psychrophilic DERAs was performed at 20 °C by sitting-drop vapor diffusion experiments, using a robotic system (Freedom EVO, Tecan). First crystals were generally observed after 1–3 days, with reservoir solutions containing 30% (w/v) PEG4000, 0.2 M lithium sulfate, 0.1 M Tris-HCl pH 8.5 (DERA_{CP}, tetragonal form), 20% (w/v) PEG1000, 0.2 M calcium acetate, 0.1 M imidazole pH 8.0 (DERA_{CP}, hexagonal form), or 30% (w/v) PEG6000, 1.0 M lithium chloride, 0.1 M sodium acetate (DERA_{SH}), and protein concentrations of 10–15 mg/ml. In case of DERA_{SH}, the initial condition was subjected to optimization, yielding well-diffracting samples with 27% (w/v) PEG6000, 1.0 M lithium chloride, 0.1 M sodium acetate, 0.1 M MES pH 6.0, and a 6.75 mg/ml protein solution. Prior to flash-cooling, crystals of DERA_{CP} were soaked in reservoir buffer containing up to 15% (v/v) glycerol; crystals of DERA_{SH} were processed in their mother liquor.

Diffraction data collection and structure determination. X-ray diffraction datasets were recorded at 100 K, using beamlines ID23-1 and ID29 of the European Synchrotron Radiation Facility (ESRF; Grenoble, France) equipped with PILATUS 6M detectors (Dectris). Data processing was performed with XDS and XSCALE⁴⁶. Initial phases for the tetragonal crystal form of DERA_{CP} (space group P4₁2₁2) were determined by molecular replacement with MOLREP⁴⁷, using chain A of DERA_{EC} (PDB ID1JCL) as a template. The asymmetric unit was found to contain two protein chains, corresponding to a Matthews coefficient of 2.69 Å³/Da and a solvent content of 54.3%. Following automated rebuilding in phenix.autobuild⁴⁸, the model was further improved by alternating reciprocal space refinement in phenix.refine⁴⁹ with rebuilding in Coot⁵⁰. The final model served as template to determine the structures of DERA_{SH} (space group C2) and the hexagonal form of DERA_{CP} (space group P6₁22) by molecular replacement. Both crystal forms contained four chains (two dimers) per asymmetric unit, with Matthews coefficients of 2.17 and 3.42 Å³/Da and solvent contents of 43.4 and 64.1%, respectively. For statistics of data collection and refinement, refer to Supplementary Table S1. Validation with MolProbity⁵¹ revealed good geometry, with all of the residues in the allowed regions of the Ramachandran plot.

Generating structural ensembles by MD simulations. To generate a structural ensemble for subsequent CNA calculations, MD simulations were performed with Amber14 using the ff14SB force field⁵². DERA wt from *E. coli* (1JCL), *T. maritima* (3R12), and *P. aerophilum* (1VCV) were obtained from the Protein Data Bank. For each protein, three independent MD simulations (initiated by slightly different equilibration temperatures of T = 299.5 K, 300.0 K, and 300.5 K) of 100 ns length at 300 K (using a time-step of 2 fs) were performed. Except for the first 5 ns, conformations were extracted every 40 ps. This

resulted in 1125 conformations for the first and 1250 for the last 50 ns. Preparation, minimization and equilibration of the system were done according to literature²². The analysis of the MD trajectories was carried out with cptraj⁵³ of AmberTools²³. The RMSD of C_α atoms with respect to the crystal structure was computed as a measure of structural similarity, as was the radius of gyration of C_α atoms as a measure of structural compactness. Furthermore, the RMSIP as a measure of the amount of overlap of the conformational subspaces of two MD trajectories was calculated as described in literature⁵⁴. The calculations were performed over the first 10 eigenvectors of a principal component analysis of the C_α atom covariance matrix of the atomic positional fluctuations²³. Prior to computing the covariance matrix, the conformations were superimposed considering only those 80% of the residues with the lowest r.m.s. fluctuations to avoid introduction of spurious correlations^{55,56}.

Constraint network analysis (CNA). Details on analyzing the thermostability of DERA with CNA are described in Supplementary Methods.

References

- Egorova, K. & Antranikian, G. Industrial relevance of thermophilic archaea. *Curr. Opin. Microbiol.* **8**, 649–655 (2005).
- Vieille, C. & Zeikus, G. J. Hyperthermophilic enzymes: sources, uses, and molecular mechanisms for thermostability. *Microbiol. Mol. Biol. Rev.* **65**, 1–43 (2001).
- Chain, P. S. *et al.* Genomics. Genome project standards in a new era of sequencing. *Science* **326**, 236–237 (2009).
- Zhou, X. X., Wang, Y. B., Pan, Y. J. & Li, W. F. Differences in amino acids composition and coupling patterns between mesophilic and thermophilic proteins. *Amino Acids* **34**, 25–33 (2008).
- Byun, J. S. *et al.* Crystal structure of hyperthermophilic esterase EstE1 and the relationship between its dimerization and thermostability properties. *BMC Struct. Biol.* **7**, 47 (2007).
- Li, W. T., Shriver, J. W. & Reeve, J. N. Mutational analysis of differences in thermostability between histones from mesophilic and hyperthermophilic archaea. *J. Bacteriol.* **182**, 812–817 (2000).
- Feller, G. & Gerday, C. Psychrophilic enzymes: Hot topics in cold adaptation. *Nat. Rev. Microbiol.* **1**, 200–208 (2003).
- Collins, T., D'Amico, S., Marx, J. C., Feller, G. & Gerday, C. *Cold-adapted enzymes*, 165–179 (2007). In Gerday, C., Glansdorff, N. (ed), *Physiology and Biochemistry of Extremophiles*, ASM Press, Washington, DC. doi: 10.1128/9781555815813.ch13.
- Feller, G. Psychrophilic enzymes: from folding to function and biotechnology. *Scientifica (Cairo)* **2013**, 512840 (2013).
- Struvay, C. & Feller, G. Optimization to low temperature activity in psychrophilic enzymes. *Int. J. Mol. Sci.* **13**, 11643–11665 (2012).
- Tozzi, M. G., Camici, M., Mascia, L., Sgarrella, F. & Ippata, P. L. Pentose phosphates in nucleoside interconversion and catabolism. *FEBS J.* **273**, 1089–1101 (2006).
- Heine, A. *et al.* Observation of covalent intermediates in an enzyme mechanism at atomic resolution. *Science* **294**, 369–374 (2001).
- Barbas, C. F., Wang, Y. F. & Wong, C. H. Deoxyribose-5-phosphate aldolase as a synthetic catalyst. *J. Am. Chem. Soc.* **112**, 2013–2014 (1990).
- Feron, G., Mauvais, G., Martin, F., Semon, E. & Blin-Perrin, C. Microbial production of 4-hydroxybenzylidene acetone, the direct precursor of raspberry ketone. *Lett. Appl. Microbiol.* **45**, 29–35 (2007).
- Sakuraba, H. *et al.* The first crystal structure of archaeal aldolase. Unique tetrameric structure of 2-deoxy-d-ribose-5-phosphate aldolase from the hyperthermophilic archaea *Aeropyrum pernix*. *J. Biol. Chem.* **278**, 10799–10806 (2003).
- Lokanath, N. K. *et al.* Structure of aldolase from *Thermus thermophilus* HB8 showing the contribution of oligomeric state to thermostability. *Acta Crystallogr. Sect. D. Biol. Crystallogr.* **60**, 1816–1823 (2004).
- Sakuraba, H. *et al.* Sequential aldol condensation catalyzed by hyperthermophilic 2-deoxy-D-ribose-5-phosphate aldolase. *Appl. Environ. Microbiol.* **73**, 7427–7434 (2007).
- Jacobs, D. J., Rader, A. J., Kuhn, L. A. & Thorpe, M. F. Protein flexibility predictions using graph theory. *Proteins.* **44**, 150–165 (2001).
- Pfleger, C., Rathi, P. C., Klein, D. L., Radestock, S. & Gohlke, H. Constraint network analysis (CNA): A python software package for efficiently linking biomacromolecular structure, flexibility, (thermo-)stability, and function. *J. Chem. Inf. Model.* **53**, 1007–1015 (2013).
- Jacobs, D. J. & Thorpe, M. F. Generic rigidity percolation: The pebble game. *Phys. Rev. Lett.* **75**, 4051–4054 (1995).
- Radestock, S. & Gohlke, H. Exploiting the link between protein rigidity and thermostability for data-driven protein engineering. *Eng. Life Sci.* **8**, 507–522 (2008).
- Rathi, P. C., Radestock, S. & Gohlke, H. Thermostabilizing mutations preferentially occur at structural weak spots with a high mutation ratio. *J. Biotechnol.* **159**, 135–144 (2012).
- Amadei, A., Linssen, A. B. M. & Berendsen, H. J. C. Essential dynamics of proteins. *Proteins-Structure Function and Genetics* **17**, 412–425 (1993).
- Gromiha, M. M., Oobatake, M. & Sarai, A. Important amino acid properties for enhanced thermostability from mesophilic to thermophilic proteins. *Biophys. Chem.* **82**, 51–67 (1999).
- Radestock, S. & Gohlke, H. Protein rigidity and thermophilic adaptation. *Proteins: Struct. Funct. Bioinf.* **79**, 1089–1108 (2011).
- Rathi, P. C., Jaeger, K. E. & Gohlke, H. Structural rigidity and protein thermostability in variants of lipase A from *Bacillus subtilis*. *PLOS One*, **10**(7), e0130289 (2015).
- Hazes, B. & Dijkstra, B. W. Model-building of disulfide bonds in proteins with known 3-dimensional structure. *Protein Eng.* **2**, 119–125 (1988).
- Wang, Z. & Moulton, J. SNPs, protein structure, and disease. *Hum. Mutat.* **17**, 263–270 (2001).
- Höcker, B., Jürgens, C., Wilmanns, M. & Sterner, R. Stability, catalytic versatility and evolution of the (β_α)₈-barrel fold. *Curr. Opin. Biotechnol.* **12**, 376–381 (2001).
- Wierenga, R. K. The TIM-barrel fold: a versatile framework for efficient enzymes. *FEBS Lett.* **492**, 193–198 (2001).
- Merz, A. *et al.* Improving the catalytic activity of a thermophilic enzyme at low temperatures. *Biochemistry* **39**, 880–889 (2000).
- Miyazaki, K. *et al.* Thermal stabilization of *Bacillus subtilis* family-11 xylanase by directed evolution. *J. Biol. Chem.* **281**, 10236–10242 (2006).
- Wei, J. S., Zhou, Y., Xu, T. & Lu, B. R. Rational design of catechol-2, 3-dioxygenase for improving the enzyme characteristics. *Appl. Biochem. Biotechnol.* **162**, 116–126 (2010).
- Takagi, H., Hirai, K., Wada, M. & Nakamori, S. Enhanced thermostability of the single-cys mutant subtilisin E under oxidizing conditions. *J. Biochem.* **128**, 585–589 (2000).

35. Marianayagam, N. J., Sunde, M. & Matthews, J. M. The power of two: protein dimerization in biology. *Trends Biochem. Sci.* **29**, 618–625 (2004).
36. Cho, C. M., Mulchandani, A. & Chen, W. Bacterial cell surface display of organophosphorus hydrolase for selective screening of improved hydrolysis of organophosphate nerve agents. *Appl. Environ. Microbiol.* **68**, 2026–2030 (2002).
37. Feller, G. Molecular adaptations to cold in psychrophilic enzymes. *Cell. Mol. Life Sci.* **60**, 648–662 (2003).
38. Xie, B. B. *et al.* Cold adaptation of zinc metalloproteases in the thermolysin family from deep sea and arctic sea ice bacteria revealed by catalytic and structural properties and molecular dynamics: new insights into relationship between conformational flexibility and hydrogen bonding. *J. Biol. Chem.* **284**, 9257–9269 (2009).
39. Papaleo, E., Olufsen, M., De Gioia, L. & Brandsdal, B. O. Optimization of electrostatics as a strategy for cold-adaptation: A case study of cold- and warm-active elastases. *J. Mol. Graph. Model.* **26**, 93–103 (2007).
40. Papaleo, E., Riccardi, L., Villa, C., Fantucci, P. & De Gioia, L. Flexibility and enzymatic cold-adaptation: A comparative molecular dynamics investigation of the elastase family. *BBA-Proteins Proteom.* **1764**, 1397–1406 (2006).
41. Tiberti, M. & Papaleo, E. Dynamic properties of extremophilic subtilisin-like serine-proteases. *J. Struct. Biol.* **174**, 69–83 (2011).
42. Papaleo, E., Renzetti, G., Invernizzi, G. & Asgerisson, B. Dynamics fingerprint and inherent asymmetric flexibility of a cold-adapted homodimeric enzyme. A case study of the *Vibrio* alkaline phosphatase. *BBA-Gen. Subjects* **1830**, 2970–2980 (2013).
43. Kullartz, I. & Pietruszka, J. Cloning and characterisation of a new 2-deoxy-D-ribose-5-phosphate aldolase from *Rhodococcus erythropolis*. *J. Biotechnol.* **161**, 174–180 (2012).
44. Follo, C. & Isidorol, C. A fast and simple method for simultaneous mixed site-specific mutagenesis of a wide coding sequence. *Biotechnol. Appl. Biochem.* **49**, 175–183 (2008).
45. Bradford, M. M. A rapid and sensitive method for the quantitation of microgram quantities of protein utilizing the principle of protein-dye binding. *Anal. Biochem.* **72**, 248–254 (1976).
46. Kabsch, W. XDS *Acta Crystallogr. Sect. D-Biol. Crystallogr.* **66**, 125–132 (2010).
47. Vagin, A. & Teplyakov, A. MOLREP: an automated program for molecular replacement. *J. Appl. Crystallogr.* **30**, 1022–1025 (1997).
48. Terwilliger, T. C. *et al.* Iterative model building, structure refinement and density modification with the PHENIX AutoBuild wizard. *Acta Crystallogr. Sect. D-Biol. Crystallogr.* **64**, 61–69 (2008).
49. Adams, P. D. *et al.* PHENIX: a comprehensive python-based system for macromolecular structure solution. *Acta Crystallogr. Sect. D-Biol. Crystallogr.* **66**, 213–221 (2010).
50. Emsley, P., Lohkamp, B., Scott, W. G. & Cowtan, K. Features and development of Coot. *Acta Crystallogr. Sect. D-Biol. Crystallogr.* **66**, 486–501 (2010).
51. Chen, V. B. *et al.* MolProbity: all-atom structure validation for macromolecular crystallography. *Acta Crystallogr. Sect. D-Biol. Crystallogr.* **66**, 12–21 (2010).
52. Amber development team (2015). AMBER 2015, University of California, San Francisco, USA. URL <http://ambermd.org/>.
53. Roe, D. R. & Cheatham, T. E. PTRAJ and CPPTRAJ: Software for processing and analysis of molecular dynamics trajectory data. *J. Chem. Theory Comput.* **9**, 3084–3095 (2013).
54. Tiwari, S. P. *et al.* WEBnm@ v2.0: Web server and services for comparing protein flexibility. *BMC Bioinformatics* **15**, 427 (2014).
55. van Gunsteren, W. F., Hunenberger, P. H., Mark, A. E., Smith, P. E. & Tironi, I. G. Computer-simulation of protein motion. *Comput. Phys. Commun.* **91**, 305–319 (1995).
56. Karplus, M. & Ichiye, T. Comment on a “fluctuation and cross correlation analysis of protein motions observed in nanosecond molecular dynamics simulations”. *J. Mol. Biol.* **263**, 120–122 (1996).
57. Zhao, J. S., Manno, D., Leggiadro, C., O’Neil, D. & Hawari, J. *Shewanella halifaxensis* sp. nov., a novel obligately respiratory and denitrifying psychrophile. *Int. J. Syst. Evol. Microbiol.* **56**, 205–212 (2006).
58. Huber, R. *et al.* *Thermotoga maritima* sp. nov. represents a new genus of unique extremely thermophilic eubacteria growing up to 90°C. *Arch. Microbiol.* **144**, 324–333 (1986).
59. Volk, P. *et al.* *Pyrobaculum aerophilum* sp. nov., a novel nitrate-reducing hyperthermophilic archaeum. *Appl. Environ. Microbiol.* **59**, 2918–2926 (1993).
60. Methe, B. A. *et al.* The psychrophilic lifestyle as revealed by the genome sequence of *Colwellia psychrerythraea* 34H through genomic and proteomic analyses. *Proc. Natl. Acad. Sci. USA* **102**, 10913–10918 (2005).

Acknowledgements

We are grateful to Dr. Christopher Pflieger for his support in constraint network analysis and Jennifer Klug for supporting cloning and mutagenesis. Generous gifts of genomic DNA from *S. halifaxensis* by Dr. Filip Kovacic (IMET, Heinrich-Heine-Universität Düsseldorf) are greatly appreciated. We thank Prof. Dr. Dieter Willbold and Dr. Philipp Neudecker (ICS-6, Forschungszentrum Jülich GmbH) for fruitful discussions. Our research was supported by the Deutsche Forschungsgemeinschaft, the Heinrich-Heine-Universität Düsseldorf (scholarship within the iGRASPseed-Graduate Cluster for M.D.), and the Forschungszentrum Jülich GmbH. The scientific activities of the Bioeconomy Science Center were financially supported by the Ministry of Innovation, Science and Research within the framework of the NRW-Strategieprojekt BioSC (No. 313/323-400-002 13).

Author Contributions

M.D. and J.P. conceived the project; M.D. and T.C. designed the mutants; M.D. cloned, purified and characterized the enzymes; C.B. developed the screening method for enantiomeric excess determination and synthesized the reference compounds; O.H.W. with assistance from M.D. and J.B. crystallized the enzymes and determined the structures; M.D. performed computational studies with assistance from H.G.; the manuscript was drafted by M.D. and finalized with contributions from all authors; H.G. and J.P. supervised research.

Additional Information

Supplementary information accompanies this paper at <http://www.nature.com/srep>

Competing financial interests: The authors declare no competing financial interests.

How to cite this article: Dick, M. *et al.* Trading off stability against activity in extremophilic aldolases. *Sci. Rep.* **6**, 17908; doi: 10.1038/srep17908 (2016).



This work is licensed under a Creative Commons Attribution 4.0 International License. The images or other third party material in this article are included in the article's Creative Commons license, unless indicated otherwise in the credit line; if the material is not included under the Creative Commons license, users will need to obtain permission from the license holder to reproduce the material. To view a copy of this license, visit <http://creativecommons.org/licenses/by/4.0/>